BMC Biology

RESEARCH

Open Access

Long-term in vivo immune tracking nanoplatform based on Ag_2S quantum dots for the photothermal immunotherapy of breast cancer

Jielin Wang[1,2,3*], Zilu Huang[4], Yongbo Wu[1,2], Xiaofang Jiang[1,2], Yanhong Ji[1,2], Kevin Braeckmans[3], Meng Wang[5], Lin Wang[6], Wei R. Chen[6], Yunfei Xia[4*], Zhilie Tang[1,2*] and Xiaozhi Xu[1,2*]

Abstract

Background Photothermal immunotherapy, as a promising technique in cancer treatment, offering precise eradication of tumor tissue, minimal adverse effects, and reduced risk of recurrence and metastasis. However, due to the instability of tracer function after photothermal immunotherapy, the long-term in vivo tracing is still a significant challenge, thereby greatly impeding the comprehensive assessment of immune response and drug delivery outcomes.

Results Here, we successfully demonstrated the feasibility of stable long-term in vivo immune tracking of photothermal immunodiagnosis and immunotherapy for breast cancer. The biocompatible and stable Ag_2S quantum dots, with an average size of 3.8 nm, were coated with ovalbumin (OVA) and loaded with immune adjuvant imiquimod (R837). This synthesized Ag_2S@OVA-R837 nanovaccine exhibited an excellent photothermal response upon near-infrared irradiation at 808 nm and effectively activated dendritic cells. In an in vivo breast tumor mouse model, we demonstrated that this nanoplatform, in combination with laser treatment, significantly improved long-term survival rates, reduced tumor size, and elicited robust immune responses.

Conclusions The results support that Ag_2S@OVA-R837 is a promising photothermal immunotherapy (PIT) tracer nanoplatform to feedback immunoefficacy of therapeutics and holds great promise for precise treatment and diagnosis of malignant tumors, providing a novel avenue for visualizing the in vivo distribution and trafficking of functional therapeutics.

Keywords Ag_2S quantum dots, Photothermal immunotherapy, Long-term tracking

*Correspondence:
Jielin Wang
wang@m.scnu.edu.cn
Yunfei Xia
xiayf@sysucc.org.cn
Zhilie Tang
tangzhl@scnu.edu.cn
Xiaozhi Xu
xiaozhixu@scnu.edu.cn
Full list of author information is available at the end of the article

Background

Cancer has emerged as one of the leading causes of mortality worldwide [1, 2], with a recent report indicating 19.3 million new cases diagnosed across 185 countries recently [2]. Therefore, cancer therapy remains a crucial research topic in biomedical research. Current treatment strategies primarily include surgery, radiotherapy, chemotherapy, and endocrine therapy, during which the balance between effectively killing tumor cells and minimizing damage to healthy tissue is critical. Additionally, the traditional therapies often struggle to completely eradicate tumor cells, leading to significant challenges with recurrence and metastasis significant challenges.

In the rapidly advancing field of cancer therapeutics, photothermal nanomaterials exhibit significant potential by enabling targeted photothermal therapy (PTT) while also facilitating the delivery of anticancer agents or immunostimulants [3–13]. These advances represent a new frontier in combating various types of cancers such as melanoma, colon cancer, and human papillomavirus -associated malignancies [14]. Over the past few years, single-walled carbon nanotubes (SWNTs), black phosphorus nanoparticles [15–18], gold nanorods (GNRs) [19–21], and iron oxide nanoparticles [22] have been demonstrated as effective contrast agents for multimodal imaging techniques such as magnetic resonance imaging (MRI) [22] and computed tomography (CT) [23]. However, these nanomaterials often face limitations, such as reduced imaging capabilities or weakened signals after PTT process, posing significant difficulties for long-term in vivo tracking [24–30]. This issue is particularly critical when assessing drug delivery and efficacy outcomes, highlighting the need for novel photothermal materials to drive further advancements in PTT applications.

Among various candidate materials, quantum dots (QDs) have emerged as promising candidates for in vivo fluorescence probes due to their stable near-infrared (NIR)-I excitation and NIR-II fluorescence emission, which enable deep tissue penetration in clinical optical imaging [16, 31–33]. Ag_2S QDs stand out because of their cost-effectiveness, high biocompatibility, and robust fluorescence stability. Ongoing studies on Ag_2S QDs are currently focused on their synthesis, fluorescence properties, and therapeutical functionalities, such as self-fluorescent Ag_2S materials [34], excitation and emission properties of Ag_2S QD [35], biocompatibility during photothermal therapy [36, 37], and chiral Ag_2S functional drugs [38] for therapeutic applications. Studies evaluating Ag_2S QDs' long-term in vivo immune tracking remain scarce. Since silver sulfide quantum dots offer a well balance between photothermal and fluorescent stability, making them effective in vivo tracers for a dynamic physical feedback of immune evaluation after immunoactivation functionalization.

In this study, we developed Ag_2S@OVA-R837 nanovaccines by combining Ag_2S QDs with ovalbumin (OVA) and imiquimod (R837) for the treatment of breast cancer using photothermal immunotherapy. In addition, the long-term monitoring of these nanovaccines' in vivo distribution was achieved using NIR-I excitation and NIR-II fluorescence imaging techniques, which enhanced their potential for further investigation and provided a visible means for auxiliary analysis. Our investigation involved synthesizing and characterizing the Ag_2S@OVA-R837 nanovaccines, followed by evaluating their photothermal capabilities and immunostimulatory effects in vitro using mouse 4T1 breast cancer cells and DC2.4 dendritic cells, respectively. The efficacy of Ag_2S@OVA-R837 in photothermal immunotherapy was evaluated in murine breast tumor model. At last, with the assistance of 808 nm laser excitation, the Ag_2S@OVA-R837 nanovaccines served as in vivo tracers, enabling visualization and tracking of the animal's immune responses to photothermal immunotherapy. Our work highlighted a long-term in vivo immune-tracking nanoplatform and has great potentials for advancing the applications of cancer photothermal immunotherapy.

Existing photothermal immunotherapy technologies have shown promising results in tumor eradication, immune activation, and the prevention of recurrence and metastasis in animal and pre-clinical studies. However, verification of these approaches often relies on late-stage biochemical detection methods and long-term safety assessments. Our work aims to develop a long-term active traceable and photothermal material that remains capable of real-time dynamic monitoring after photothermal treatment. This approach provides a novel research perspective that could accelerated the clinical development cycle of new photothermal immune therapies and breast cancer treatments.

Results

Synthesis and characterization of Ag_2S@OVA-R837

To enhance the immune activation effect, the Ag_2S QDs were synthesized and coated with the OVA antigen, a widely used antigen in immune research [39]. Afterwards, the FDA-approved immunomodulator R837, which targets Toll-like receptor 7, was loaded, creating a multimodal approach for breast cancer treatment (Fig. 1a). Transmission electron microscopy (TEM) images revealed that the Ag_2S cores possessed an average diameter of 3.8 ± 0.6 nm (Fig. 1b). Complementary x-ray photoelectron spectroscopy (XPS) measurements corroborated the chemical identity of the Ag_2S, identifying the binding energy peaks at 373.3 and 367.4 eV for Ag

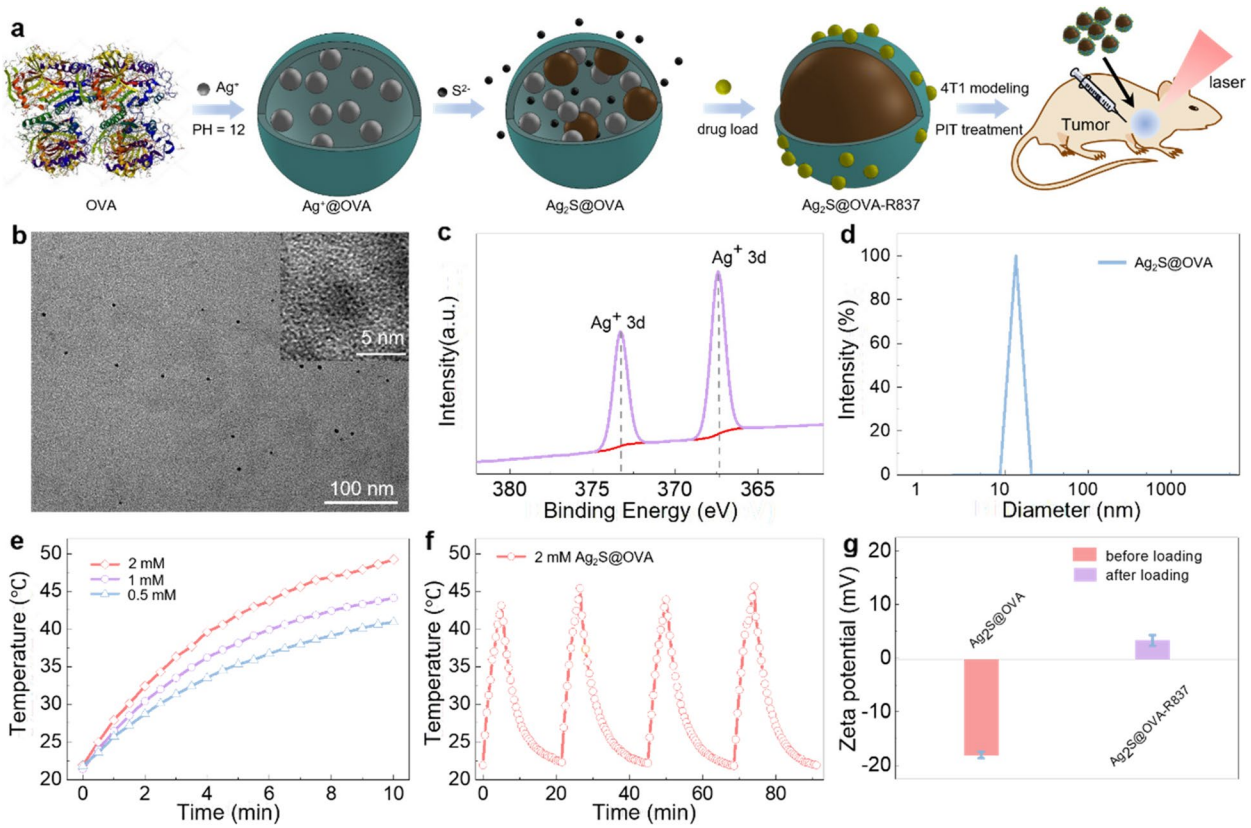

Fig. 1 Synthesis and characterization of Ag_2S@OVA-R837. **a** Schematic diagrams of the synthesis of Ag_2S@OVA-R837 for the photothermal immunotherapy of 4T1 tumor model. **b** TEM images of the Ag_2S QDs. Inset: a zoom-in image of individual Ag_2S QDs. **c** XPS spectrum of Ag_2S@OVA confirming the chemical content of Ag. **d** DLS analysis revealing the size distribution of Ag_2S@OVA nanoparticles. **e** Photothermal response curves for Ag_2S QDs at different concentrations under 10 min of laser irradiation (808 nm, 1.0 W/cm^2). **f** Repeated heating profiles for 2 mM Ag_2S@OVA over four cycles of irradiation (808 nm, 1.0 W/cm^2), demonstrating the photothermal stability. **g** Comparative zeta potential measurements of Ag_2S@OVA and Ag_2S@OVA-R837 nanoparticles

(Fig. 1c), and a peak at 162.8 eV for S (Additional file1: Fig. S1). Dynamic light scattering (DLS) analysis indicated that Ag_2S@OVA nanoparticles had an approximate size of 13.5 nm with a narrow size distribution, suggesting excellent colloidal stability in phosphate-buffered saline (PBS) at a pH of 7.4 (Fig. 1d). The broadband absorption property of Ag_2S QDs was confirmed by the ultraviolet–visible absorption spectrum (Additional file1: Fig. S2).

To assess the photothermal properties, Ag_2S@OVA solutions at varying concentrations (0.5, 1, and 2 mM Ag) were exposed to an 808 nm laser (1.0 W/cm^2) for 10 min. A concentration-dependent temperature increase can be clearly observed (Fig. 1e). The photothermal stability of Ag_2S@OVA nanoparticles (2 mM Ag) was tested over four irradiation cycles (808 nm laser, 1.0 W/cm^2, 5 min of irradiation followed by a cooling period to room temperature). The nanoparticles showed consistent photothermal effects with no observable reduction in performance (Fig. 1f). Comparison across different concentrations is provided in Additional file1: Fig. S3, which indicates that higher concentrations also maintain a stable temperature rise during the 5-min irradiation period. The electrostatic adsorption of R837 onto the Ag_2S@OVA nanoparticles was evidenced by a shift in zeta potential from -18.04 ± 0.61 mV to 3.31 ± 0.98 mV, confirming the successful formation of Ag_2S@OVA-R837 (Fig. 1g). The loading efficiency of R837 onto Ag_2S@OVA was quantified at 53.7%, using a standard calibration curve [7].

In vitro cytokine secretion detection

The cytotoxicity of Ag_2S QDs on 4T1 cells were assessed using the cell counting kit-8 (CCK-8) assay following a 24-h incubation period. The results demonstrated an absence of cytotoxicity, even at the highest concentration tested (4 mM of Ag, Fig. 2a). To further verify the safety of the materials, a hemolysis assay was conducted (Additional file1: Fig. S4). The hemolysis rates for both Ag_2S@OVA and Ag_2S@OVA-R837 were below 2%, measured at 1.45% and 0.27%, respectively. These results

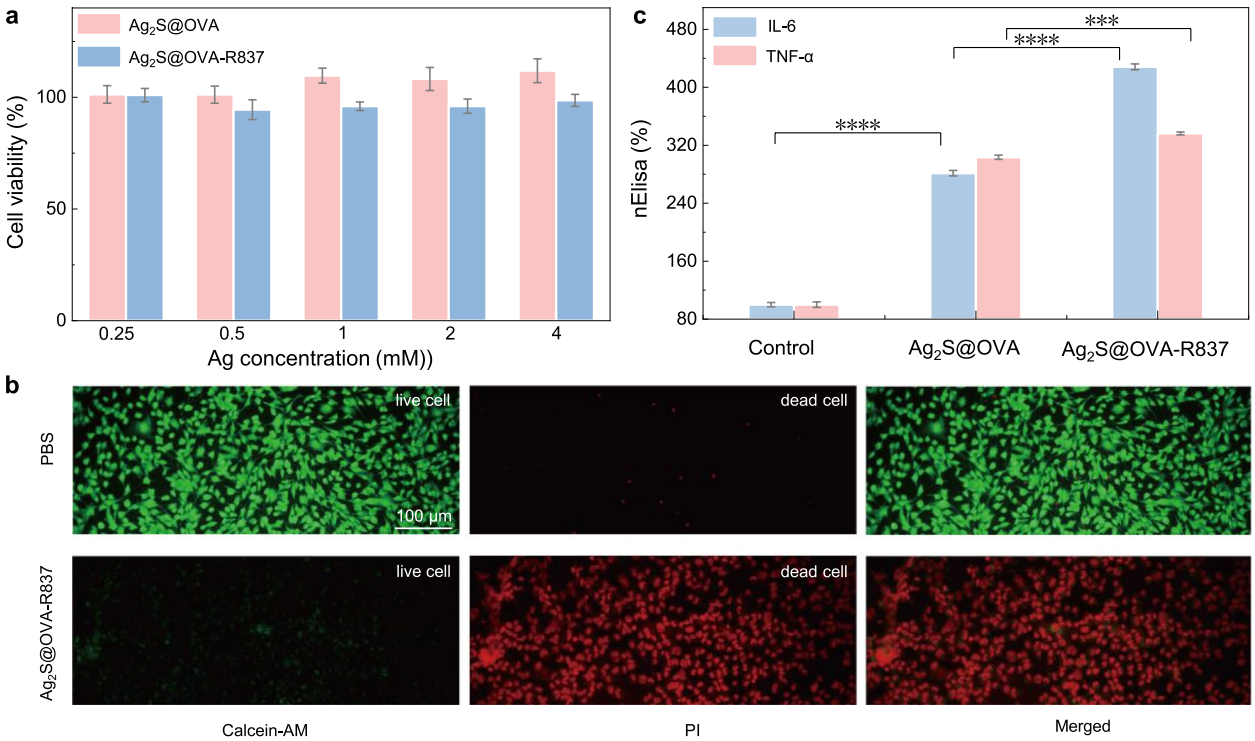

Fig. 2 In vitro cytokine secretion detection. **a** Cell viability of 4T1 cells after a 24-h incubation with different concentrations of nanoplatforms based on Ag_2S QDs. **b** Fluorescence microscopy images showcasing 4T1 cells treated with 2 mM Ag_2S@OVA-R837, followed by a 10-min irradiation with an 808 nm laser at a power density of 1.0 W/cm^2. Live cells are stained with calcein AM (green fluorescence), while dead cells are stained with propidium iodide (PI, red fluorescence). **c** Normalized ELISA results indicating the secretion levels of IL-6 and TNF-α by DC2.4 cells in response to treatment with PBS, Ag_2S@OVA, and Ag_2S@OVA-R837. Data are represented as mean ± SD ($n = 3$). Statistical significance is denoted as ns (not significant), ***$p < 0.001$, ****$p < 0.0001$, based on two-way ANOVA

demonstrated that the Ag_2S@OVA-R837 nanovaccines exhibited excellent biocompatibility.

The photothermal cytotoxic efficacy of the Ag_2S@OVA-R837 nanovaccine was evaluated on 4T1 cells subjected to 10 min of laser irradiation (808 nm, 1.0 W/cm^2). The assessment was conducted by fluorescent microscopy with live/dead staining, in comparison with a PBS control. Live cells were identified by calcein AM staining and emitted green fluorescence, while dead cells were marked by propidium iodide (PI) staining and emitted red fluorescence (Fig. 2b). The results demonstrate that Ag_2S@OVA-R837 nanoparticles, upon laser irradiation, were effective in inducing cell death in 4T1 cells, providing preliminary in vitro evidence of its potential for tumor photothermal ablation. This supports the capability of the nanovaccines for subsequent in vivo studies. Further comparison of the in vivo photothermal effect is shown in Additional file1: Fig. S5.

Dendritic cells (DCs) are pivotal as antigen-presenting cells (APCs) in T cell activation. In our experiment, DC2.4 cells were incubated with PBS, Ag_2S@OVA (2 mM Ag), and Ag_2S@OVA-R837 (2 mM Ag) for 24 h. The secretion levels of the cytokines interleukin 6 (IL-6) and tumor necrosis factor alpha (TNF-alpha) were measured using enzyme-linked immunosorbent assay (ELISA). Notably, a significant increase in both TNF-alpha and IL-6 secretion was detected following treatment with Ag_2S@OVA, with a more pronounced elevation upon exposure to Ag_2S@OVA-R837 (Fig. 2c).

These preliminary findings indicate that Ag_2S@OVA-R837 can stimulate and enhance the immune response of APCs, thereby has a potential in activating naive T cells subsequently. This provides promising evidence for its capability to trigger immune responses in vivo, suggesting its potential as an immunotherapeutic agent.

In vivoantitumor efficacy

The in vivo antitumor efficacy of Ag_2S@OVA-R837 (intratumoral administered at 2 mM Ag per 20 g mouse) combined with laser treatment (808 nm, 1.0 W/cm^2, for 10 min) was evaluated in a murine model bearing 4T1 tumors. This treatment was compared against groups receiving Ag_2S@OVA with laser treatment, PBS with laser treatment, and an untreated control group. Over an extended study period of more than 90 days, the survival rate of mice treated with Ag_2S@OVA-R837 was the

highest at 83%, with complete tumor regression observed after 15 days (Fig. 3a–b). In contrast, mice receiving Ag_2S@OVA and PBS with laser treatments showed survival rates of 33% and 17%, respectively, while the control group exhibited the most significant tumor growth and all animals succumbed within 33 days.

Serum levels of TNF-alpha, measured via ELISA, showed a marked increase after treatment with both Ag_2S@OVA and notably Ag_2S@OVA-R837 on days one, three, and seven (Fig. 3c). IL-6 levels peaked one day after the Ag_2S@OVA-R837 treatment and then gradually declined. In mice treated with Ag_2S@OVA, IL-6 levels rose more steadily, reaching the peak on day three before diminishing (Fig. 3d).

These findings collectively suggest that the Ag_2S@OVA-R837 nanovaccines, when used in combination with PTT, effectively stimulate strong immune responses in vivo, highlighting its potential as a therapeutic strategy for cancer treatment.

Long-term in vivo immune tracking

The development of stable and anti-photobleaching NIR-II fluorescence probes is crucial for advancing tracking research. Despite their potential, Ag_2S QDs have not yet been explored as tracers for immune functionalization in vivo. The fluorescence emission spectrum of Ag_2S@OVA-R837 upon excitation at 808 nm is shown in Additional file1:Fig. S6, featuring a distinct, narrow peak centered at 1096 nm, well within the desired NIR-II spectral region. Fluorescence imaging was conducted using an 1100 nm long-pass filter to capture the emission from suspensions of both Ag_2S@OVA and Ag_2S@OVA-R837 before and after 10 min of laser irradiation (808 nm, 1.0 W/cm^2) in a dark setting. The absence of significant photobleaching suggests that these Ag_2S QDs remain stable after PTT (Fig. 4a).

To assess the potential for in vivo imaging, Ag_2S QDs were intravenously injected into healthy mice and tracked over a 3-day period. The images in Fig. 4b validate the successful in vivo visualization of the nanoparticles, with pronounced accumulation observed in the liver and intestines after 3 days. Furthermore, Ag_2S@OVA-R837 was administered to tumor-bearing mice, with subsets of mice receiving PTT treatment (10 min, 808 nm, 1.0 W/cm^2) and others not. In the absence of PTT, the Ag_2S@OVA-R837 nanovaccines were initially detectable at the

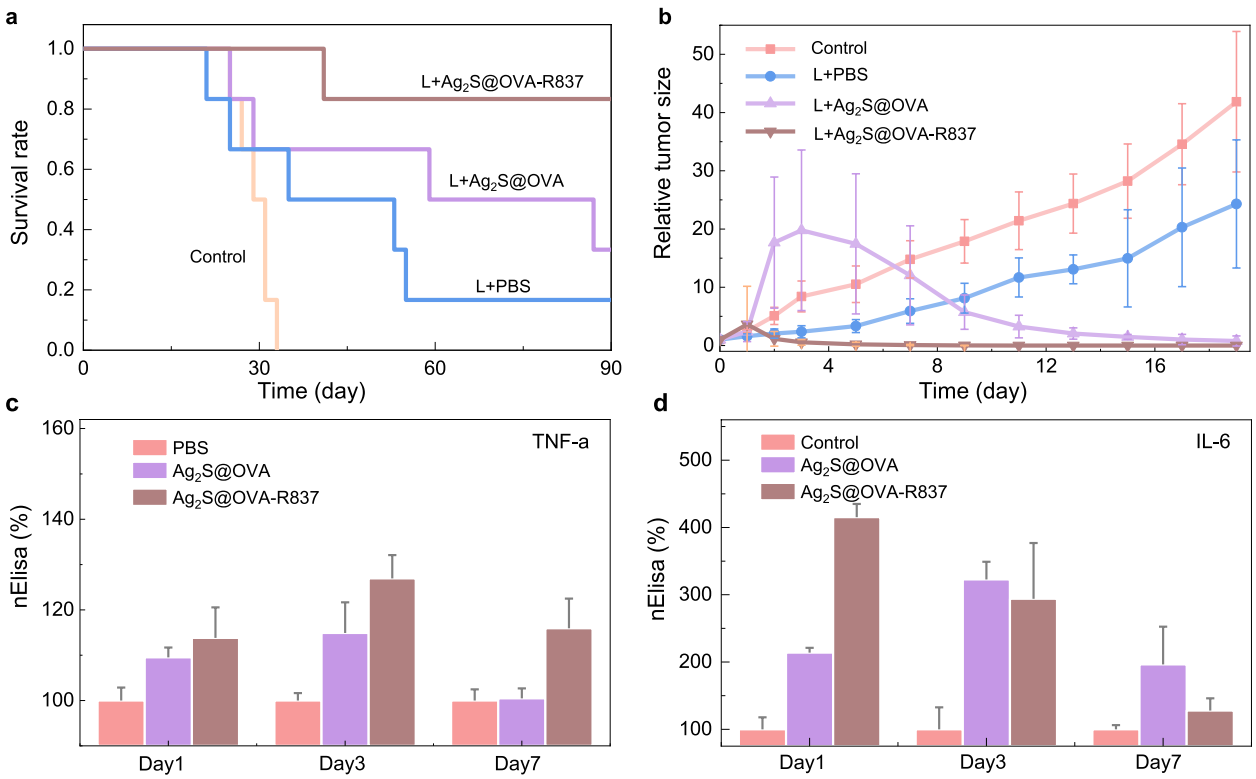

Fig. 3 In vivo antitumor efficacy. **a** Survival rates of the tumor-bearing mouse model post-treatment with PBS, Ag_2S@OVA, or Ag_2S@OVA-R837, each in combination with 10 min of laser irradiation (808 nm, 1.0 W/cm.^{2}). **b** Relative tumor volumes in BALB/c mice measured 15 days after treatment. **c** Serum TNF-α concentrations in mice at 1, 3, and 7 days post-treatment. **d** Serum IL-6 concentrations in mice at 1, 3, and 7 days post-treatment. The data for **a** and **b** are presented as mean ± SD ($n = 12$), while the results for **c** and **d** are depicted as mean ± SD ($n = 5$)

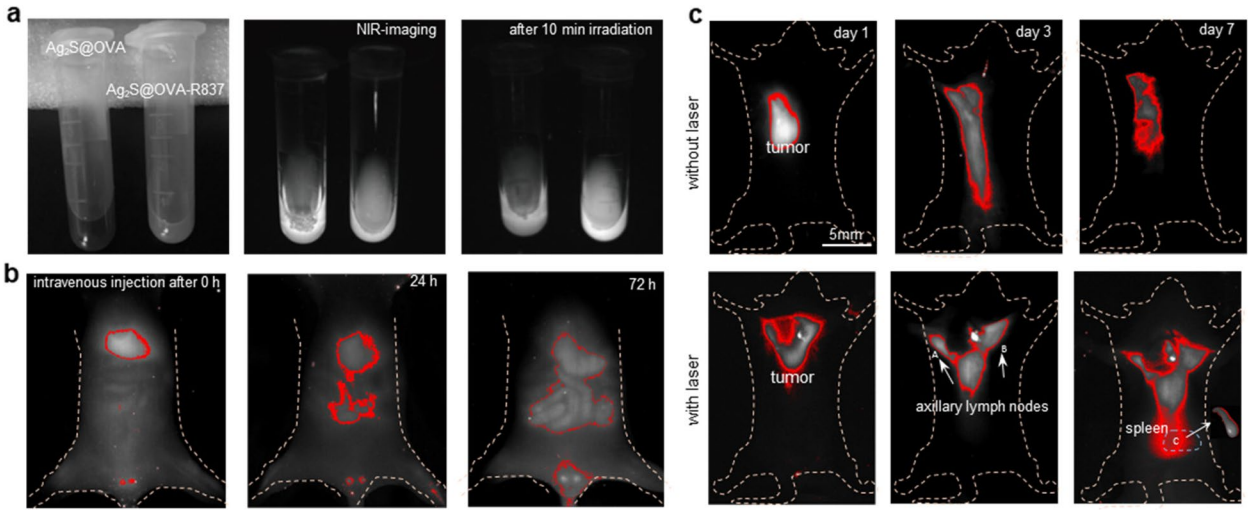

Fig. 4 Long-term in vivo immune tracking. **a** Near-infrared imaging of Ag_2S@OVA and Ag_2S@OVA-R837 pre- and post-laser irradiation. **b** NIR imaging over a period of 0–72 h in BALB/c mice post-tail vein injection with Ag_2S@OVA-R837 nanoparticles. **c**–**d** Near-infrared imaging from day 1 to day 7 in tumor-bearing BALB/c mice, without (**c**) and with (**d**) photothermal immunotherapy. A and B indicate axillary lymph nodes, while C denotes the spleen

tumor site on day 1, but the signal gradually dissipated and became undetectable over time (Fig. 4c). In contrast, PTT-treated mice not only exhibited nanoparticle localization within the tumor but also in both bilateral axillary lymph nodes, with marked visibility on day 3. By day 7 post-injection, the particles were also detectable within the spleen (Fig. 4d), indicating the possibility of inducing memory immune responses. This immune reaction was further demonstrated by the ex vivo analysis of excised axillary lymph nodes (Additional file1: Fig. S7).

Discussion

Our work introduces a new real-time dynamic feedback method for the research and development of functional therapeutics for breast cancer, which could help shorten the clinical development cycle. However, practical applications are still limited by penetration depth, and the research is still primarily focused on animal models. Further studies are required to evaluate its long-term safety and in vivo metabolism in humans. Additionally, advancements in infrared imaging and endoscopy technology are needed to enhance the impact of this approach on the development of functional therapeutics for clinical breast cancer treatment.

Conclusion

In conclusion, we have developed a versatile nanoplatform utilizing Ag_2S QDs loaded with antigen and adjuvant for synergistic photothermal and immunotherapy. Owing to the unique optical properties of silver sulfide quantum dots, they effectively balance photothermal and fluorescence stabilization functions. This makes them well-suited for long-term, real-time dynamic monitoring of in vivo biodistribution of photothermal immunofunctional therapeutics and other innovative agents. This system demonstrates remarkable in vivo tracking capabilities for over 7 days through NIR-II fluorescence imaging, even after continuous exposure to irradiation exceeding 10 min. Upon exposure to an 808 nm laser, the antitumor efficacy of our nanoplatform was validated both in vitro and in vivo, highlighting its significant potential for diagnostic and therapeutic applications. This platform involves wrapping immune antigens and loading immune adjuvants to enhance immune responses after photothermal immunotherapy. The development of this nanoplatform system holds promise for accurate treatment and post-treatment feedback of photothermal immunotherapy for malignant tumors, offering a new avenue for visualizing the in vivo distribution and trafficking of functional therapeutics.

Methods

Materials

Silver nitrate, sodium sulfide, sodium hydroxide, ovalbumin (OVA, molecular weight 44,287), Cell Counting Kit-8 (CCK-8), and imiquimod (R837) were purchased from Sigma-Aldrich. Fetal bovine serum (FBS), Roswell Park Memorial Institute (RPMI) 1640 medium, 0.25% trypsin–EDTA solution, as well as penicillin and streptomycin antibiotics were obtained from Gibco. Fluorescent dyes calcein AM and propidium iodide were supplied by Thermo Fisher Scientific.

Cell culture and experiments

In this study, 4T1 cells were used as a breast cancer model. The cells were cultured in RPMI-1640 medium supplemented with 10% FBS and 1% penicillin–streptomycin and maintained at 37 °C in a humidified incubator with 5% CO_2.

For the cytotoxicity assays, cells were incubated with Ag_2S quantum dots (QDs) for 24 h at various silver (Ag) concentrations as specified in the text. Subsequently, the cells were rinsed to eliminate any unbound particles in the solution. Thereafter, 200 μL of cell medium containing 10% Cell Counting Kit-8 (CCK-8) solution was added to each well for a 2–3 h incubation period prior to absorbance measurement. Cell viability was then calculated using the following formula: Cell viability $=(V_{test}-V_{blank})/(V_{PBS}-V_{blank})$, where "$V$" represents the absorbance values obtained from the microplate reader.

For cytotoxicity assays, 4T1 cells were incubated with Ag2S quantum dots (QDs) for 24 h at different silver (Ag) concentrations, as described in the text. After incubation, cells were washed to remove any unbound particles. Then, 200 μL of culture medium containing 10% CCK-8 solution was added to each well and incubated for 2–3 h before measuring absorbance. Cell viability was calculated using the following formula: Cell viability $=(V_{test}-V_{blank})/(V_{PBS}-V_{blank})$, where "$V$" represents the absorbance values obtained from the microplate reader.

For fluorescence imaging, cells were treated with either PBS as a control or with Ag2S QDs at a concentration of 2 mM Ag, followed by irradiation with an 808 nm laser at a power density of 1.0 W/cm^2 for 10 min. After irradiation, the cells were washed and stained with calcein AM and propidium iodide (PI) for 30 min to facilitate imaging.

Synthesis of Ag_2S@OVA-R837

To synthesize Ag2S@OVA nanoparticles, silver nitrate (AgNO3, 20 mM) was added to an ovalbumin (OVA) solution (250 mg in 9 mL water) under continuous stirring. Sodium sulfide (Na2S, 0.1 M) was then added gradually to the mixture, which was stirred overnight at 55 °C to facilitate the formation of Ag2S@OVA nanoparticles. The resulting suspension was dialyzed for 24 h using a 100 kDa cut-off membrane in a buffer solution.

To load the immunostimulant imiquimod (R837) onto the nanoparticles, R837 (0.5 mg in 1 mL methanol) was added to the Ag2S@OVA solution. The mixture was stirred overnight in an open vial to allow evaporation of any residual methanol. The final product was dialyzed with a 10-kDa cut-off membrane to remove unbound R837 and subsequently freeze-dried. The loading efficiency of R837 was quantified using UV absorption at 325 nm.

Characterization and photothermal evaluation of Ag_2S QDs

Transmission electron microscopy (TEM) was used to characterize Ag2S QDs using a JEM-2100 electron microscope (JEOL Ltd., Japan). X-ray photoelectron spectroscopy (XPS) analysis was performed with an AXIS SUPRA spectrometer (Shimadzu, Japan). The UV–Visible absorption spectrum was measured using a TU-1810 spectrophotometer (Puxitongyong, Beijing). Thermal measurements were conducted using an LE-LS-808 laser system (Feichuang, Shenzhen) with 808 nm laser irradiation, and temperature changes were detected using an infrared thermal detector. NIR-I (808 nm excitation) and NIR-II (emission at ~ 1100 nm) data were recorded using a Princeton Instrument (PI 2300).

In vitro cytokine secretion analysis (DC2.4)

DC2.4 cells, an immature dendritic cell line, were used to assess cytokine secretion. Cells were treated with PBS, Ag2S@OVA nanoparticles, or Ag2S@OVA-R837 nanovaccines for 24 h. Secretion levels of tumor necrosis factor-alpha (TNF-α) and interleukin-6 (IL-6) were quantified using enzyme-linked immunosorbent assay (ELISA) to evaluate immune response.

Animal model

Female BALB/c mice, aged 5–6 weeks, were obtained from Guangdong Medical Laboratory Animal Centre. A total of 1×10^5 4T1 cells suspended in 0.1 mL PBS were subcutaneously injected into the primary mammary gland in the thoracic region. When the tumor volume reached 100–200 mm^3 (typically 7–10 days post-inoculation), the mice were randomly divided into four groups. Each group consisted of 12 mice for long-term survival analysis and 5 mice for serum cytokine measurement.

The treatment groups were as follows: (1) PBS (100 μL) with laser exposure (1.0 W/cm^2 for 10 min), (2) Ag2S@OVA-R837 ([Ag] = 10 mM, 100 μL) with laser exposure (1.0 W/cm^2 for 10 min), (3) Ag2S@OVA ([Ag] = 2 mM, 100 μL) with laser exposure (1.0 W/cm^2 for 10 min), and (4) Ag2S@OVA-R837 ([Ag] = 2 mM, 100 μL) without laser treatment.

Serum cytokine levels were measured in 5 mice from each group at 1, 3, and 7 days post-treatment using ELISA. During the experiments, anesthesia was administered using isoflurane, and euthanasia was performed by cervical dislocation.

NIR-II in vivo tracking

NIR-II in vivo tracking was conducted using a non-invasive fluorescence imaging system equipped with an indium gallium arsenide (InGaAs) camera. Ag_2S QDs were injected via the tail vein of healthy mice and monitored for 3 days to evaluate in vivo stability and metabolic pathways.

Furthermore, Ag_2S@OVA-R837 was injected into a 4T1 tumor-bearing mouse model to investigate the in vivo biodistribution. The comparison was made between mice that received no laser treatment and those that underwent laser irradiation (1.0 W/cm^2 for 10 min) at 1, 3, and 7 days post-injection.

To assess biodistribution, Ag2S@OVA-R837 was injected into tumor-bearing mice, and comparisons were made between those with and without laser irradiation (1.0 W/cm^2 for 10 min) at 1, 3, and 7 days post-injection.

Abbreviations

OVA	Ovalbumin
PTT	Photothermal therapy
SWNTs	Single-walled carbon nanotubes
GNRs	Gold nanorods
MRI	Magnetic resonance imaging
CT	Computed tomography
QDs	Quantum dots
NIR	Near-infrared
TEM	Transmission electron microscopy
XPS	X-ray photoelectron spectroscopy
DLS	Dynamic light scattering
PBS	Phosphate-buffered saline
CCK- 8	Cell counting kit-8
PI	Propidium iodide
DCs	Dendritic cells
APCs	Antigen-presenting cells
IL- 6	Interleukin 6
TNF-alpha	Tumor necrosis factor alpha
ELISA	Enzyme-linked immunosorbent assay
InGaAs	Indium gallium arsenide

Supplementary Information

The online version contains supplementary material available at https://doi.org/10.1186/s12915-025-02215-w.

Additional file 1: Figures S1-S8. FigS1- The XPS spectrum revealing peak for S at approximately 162.2 eV. FigS2- UV-vis absorption spectrum of Ag2S@OVA. FigS3- Four thermal cycling profiles at different concentrations of Ag2S QDs. FigS4- Results of the hemolysis assay. FigS5- Monitoring the highest temperature of different groups. FigS6- Fluorescence emission spectrum upon excitation at 808 nm. FigS7- The ex vivo analysis of excised axillary lymph nodes. FigS8- The diagram illustrating the treatment process of Ag2S@OVA-R837 in vivo

Acknowledgements

J.W. is sincerely thankful for the financial assistance provided by the Innovation Project of the Graduate School of South China Normal University. Our appreciation extends to the University of Central Oklahoma (Zhou Benqin) and Sun Yat-sen University for their support with the cell experiments. We are also grateful to Ghent University for their valuable suggestions and language revisions and to South China University of Technology (Wu Xiao) and Fudan University (Zhao Mengyao) for their support with NIR-II in vivo tracking.

Authors' contributions

JLW completed the entirety of the experimental work, encompassing material synthesis, cell culture, in vivo imaging experiments, and the preparation of the initial draft manuscript. ZLH and MW provided support for the immunological experiments. YBW and XFJ contributed material and technical support for imaging. YHJ provided the Biotechnology Training support. KB and LW assisted with part of the manuscript review and editing process. YFX, ZLT, and XZX, as corresponding authors, provided guidance, supervision, and additional support in writing and editing the manuscript. All authors read and approved the final manuscript.

Funding

We would like to express our gratitude to the financial support received from the Guangdong Basic and Applied Basic Research Foundation (Grant No. 2022 A1515110348), Guangdong Natural Science Foundation (2022 A1515011420), the China Postdoctoral Science Foundation (Grant No. 2022M711223), and the National Natural Science Foundation of China (Grant No. 61575067, 12322406 and 52102043).

Data availability

No datasets were generated or analysed during the current study.

Declarations

Ethics approval and consent to participate

This article contains experiments with animals that were approved by the Ethics Committee from South China Normal University (1129093).

Consent for publication

Not applicable.

Competing interests

The authors declare no competing interests.

Author details

[1]Guangdong Basic Research Center of Excellence for Structure and Fundamental Interactions of Matter, Guangdong Provincial Key Laboratory of Quantum Engineering and Quantum Materials, School of Physics, South China Normal University, Guangzhou 510006, China. [2]Frontier Research Institute for Physics, Guangdong-Hong Kong Joint Laboratory of Quantum Matter, South China Normal University, Guangzhou 510006, China. [3]Laboratory of General Biochemistry and Physical Pharmacy, Faculty of Pharmaceutical Sciences, Ghent University, Ottergemsesteenweg 460, Ghent 9000, Belgium. [4]State Key Laboratory of Oncology in South China, Sun Yat-Sen University Cancer Center, Guangzhou 510060, China. [5]Shenzhen University Medical School, Shenzhen University, Shenzhen 518055, China. [6]Stephenson School of Biomedical Engineering, University of Oklahoma, Norman, OK 73019, USA.

Received: 11 September 2024 Accepted: 14 April 2025
Published online: 28 April 2025

References

1. Sung H, Ferlay J, Siegel RL, Laversanne M, Soerjomataram I, Jemal A, et al. Global Cancer Statistics 2020: GLOBOCAN Estimates of Incidence and Mortality Worldwide for 36 Cancers in 185 Countries. CA: a cancer journal for clinicians. 2021;71(3):209–49.
2. Chhikara B, Parang K. Global Cancer Statistics 2022: The Trends Projection Analysis. Chemical Biology Letters. 2022;10:451.
3. Tao Y, Ju E, Liu Z, Dong K, Ren J, Qu X. Engineered, self-assembled near-infrared photothermal agents for combined tumor immunotherapy and chemo-photothermal therapy. Biomaterials. 2014;35(24):6646–56.
4. Chen Q, Xu L, Liang C, Wang C, Peng R, Liu Z. Photothermal therapy with immune-adjuvant nanoparticles together with checkpoint blockade for effective cancer immunotherapy. Nat Commun. 2016;7(1):1–13.
5. Ou W, Byeon JH, Thapa RK, Ku SK, Yong CS, Kim JO. Plug-and-Play nanorization of coarse black phosphorus for targeted chemo-photoimmunotherapy of colorectal cancer. ACS Nano. 2018;12(10):10061–74.

6. Zong S, Wang L, Yang Z, Wang H, Wang Z, Cui Y. Black Phosphorus-Based Drug Nanocarrier for Targeted and Synergetic Chemophotothermal Therapy of Acute Lymphoblastic Leukemia. ACS Appl Mater Interfaces. 2019;11(6):5896–902.
7. Xu J, Xu L, Wang C, Yang R, Zhuang Q, Han X, et al. Near-Infrared-Triggered Photodynamic Therapy with Multitasking Upconversion Nanoparticles in Combination with Checkpoint Blockade for Immunotherapy of Colorectal Cancer. ACS Nano. 2017;11(5):4463–74.
8. Sun R, Liu M, Lu J, Chu B, Yang Y, Song B, et al. Bacteria loaded with glucose polymer and photosensitive ICG silicon-nanoparticles for glioblastoma photothermal immunotherapy. Nat Commun. 2022;13(1):5127.
9. Chen Q, Xu L, Liang C, Wang C, Peng R, Liu Z. Photothermal therapy with immune-adjuvant nanoparticles together with checkpoint blockade for effective cancer immunotherapy. Nat Commun. 2016;7(1):13193.
10. Nam J, Son S, Ochyl LJ, Kuai R, Schwendeman A, Moon JJ. Chemophotothermal therapy combination elicits anti-tumor immunity against advanced metastatic cancer. Nat Commun. 2018;9(1):1074.
11. Jiang Y, Huang J, Xu C, Pu K. Activatable polymer nanoagonist for second near-infrared photothermal immunotherapy of cancer. Nat Commun. 2021;12(1):742.
12. Song C, Zhang X, Cao Z, Wei Z, Zhou M, Wang Y, et al. Regulating tumor cholesterol microenvironment to enhance photoimmunotherapy in oral squamous cell carcinoma. Chem Eng J. 2023;462: 142160.
13. Song C, Wu X, Wang J, Liu R, Zhao Y. Photosensitizer-immunotherapy integrated microneedles for preventing tumor recurrence and metastasis. Nano Today. 2023;51: 101913.
14. Zhou H, Zeng X, Li A, Zhou W, Tang L, Hu W, et al. Upconversion NIR-II fluorophores for mitochondria-targeted cancer imaging and photothermal therapy. Nat Commun. 2020;11(1):6183.
15. Sun C, Wen L, Zeng J, Wang Y, Sun Q, Deng L, et al. One-pot solventless preparation of PEGylated black phosphorus nanoparticles for photoacoustic imaging and photothermal therapy of cancer. Biomaterials. 2016;91:81–9.
16. Wang R, Zhou L, Wang W, Li X, Zhang F. In vivo gastrointestinal drug-release monitoring through second near-infrared window fluorescent bioimaging with orally delivered microcarriers. Nat Commun. 2017;8(1):14702.
17. Shao J, Xie H, Huang H, Li Z, Sun Z, Xu Y, et al. Biodegradable black phosphorus-based nanospheres for in vivo photothermal cancer therapy. Nat Commun. 2016;7(1):12967.
18. Deng L, Xu Y, Sun C, Yun B, Sun Q, Zhao C, et al. Functionalization of small black phosphorus nanoparticles for targeted imaging and photothermal therapy of cancer. Science Bulletin. 2018;63(14):917–24.
19. Rastinehad AR, Anastos H, Wajswol E, Winoker JS, Sfakianos JP, Doppalapudi SK, et al. Gold nanoshell-localized photothermal ablation of prostate tumors in a clinical pilot device study. Proc Natl Acad Sci. 2019;116(37):18590–6.
20. Kim C, Cho EC, Chen J, Song KH, Au L, Favazza C, et al. In vivo molecular photoacoustic tomography of melanomas targeted by bioconjugated gold nanocages. ACS Nano. 2010;4(8):4559–64.
21. Xu G, Li C, Chi C, Wu L, Sun Y, Zhao J, et al. A supramolecular photosensitizer derived from an Arene-Ru(II) complex self-assembly for NIR activated photodynamic and photothermal therapy. Nat Commun. 2022;13(1):3064.
22. Chen H, Burnett J, Zhang F, Zhang J, Paholak H, Sun D. Highly crystallized iron oxide nanoparticles as effective and biodegradable mediators for photothermal cancer therapy. Journal of Materials Chemistry B. 2014;2(7):757–65.
23. Huang X, El-Sayed IH, Qian W, El-Sayed MA. Cancer cell imaging and photothermal therapy in the near-infrared region by using gold nanorods. J Am Chem Soc. 2006;128(6):2115–20.
24. Li Z, Liang P-Z, Xu L, Zhang X-X, Li K, Wu Q, et al. In situ orderly self-assembly strategy affording NIR-II-J-aggregates for in vivo imaging and surgical navigation. Nat Commun. 2023;14(1):1843.
25. Grandjean CL, Garcia Z, Lemaître F, Bréart B, Bousso P. Imaging the mechanisms of anti-CD20 therapy in vivo uncovers spatiotemporal bottlenecks in antibody-dependent phagocytosis. Sci adv. 2021;7(8):eabd6167.
26. Chen M, Feng Z, Fan X, Sun J, Geng W, Wu T, et al. Long-term monitoring of intravital biological processes using fluorescent protein-assisted NIR-II imaging. Nat Commun. 2022;13(1):6643.
27. Li B, Wang W, Zhao L, Wu Y, Li X, Yan D, et al. Photothermal therapy of tuberculosis using targeting pre-activated macrophage membrane-coated nanoparticles. Nat Nanotechnol. 2024;19(6):834–45.
28. Li X, Yong T, Wei Z, Bie N, Zhang X, Zhan G, et al. Reversing insufficient photothermal therapy-induced tumor relapse and metastasis by regulating cancer-associated fibroblasts. Nat Commun. 2022;13(1):2794.
29. Shi Z, Luo M, Huang Q, Ding C, Wang W, Wu Y, et al. NIR-dye bridged human serum albumin reassemblies for effective photothermal therapy of tumor. Nat Commun. 2023;14(1):6567.
30. Song C, Ran J, Wei Z, Wang Y, Chen S, Lin L, et al. Organic Near-Infrared-II Nanophotosensitizer for Safe Cancer Phototheranostics and Improving Immune Microenvironment against Metastatic Tumor. ACS Appl Mater Interfaces. 2021;13(3):3547–58.
31. Shemetov AA, Monakhov MV, Zhang Q, Canton-Josh JE, Kumar M, Chen M, et al. A near-infrared genetically encoded calcium indicator for in vivo imaging. Nat Biotechnol. 2021;39(3):368–77.
32. Liu Y, Liu H, Yan H, Liu Y, Zhang J, Shan W, et al. Aggregation-Induced Absorption Enhancement for Deep Near-Infrared II Photoacoustic Imaging of Brain Gliomas In Vivo. Adv Sci. 2019;6(8):1801615.
33. Dou WT, Han HH, Sedgwick AC, Zhu GB, Zang Y, Yang XR, et al. Fluorescent probes for the detection of disease-associated biomarkers. Sci Bull (Beijing). 2022;67(8):853–78.
34. Afshari MJ, Li C, Zeng J, Cui J, Wu S, Gao M. Self-illuminating NIR-II bioluminescence imaging probe based on silver sulfide quantum dots. ACS Nano. 2022;16(10):16824–32.
35. Du Y, Xu B, Fu T, Cai M, Li F, Zhang Y, et al. Near-infrared photoluminescent Ag2S quantum dots from a single source precursor. J Am Chem Soc. 2010;132(5):1470–1.
36. Yang T, Tang Ya, Liu L, Lv X, Wang Q, Ke H, et al. Size-Dependent Ag2S Nanodots for Second Near-Infrared Fluorescence/Photoacoustics Imaging and Simultaneous Photothermal Therapy. Acs Nano. 2017;11(2):1848–57.
37. Han R, Xiao Y, Yang Q, Pan M, Hao Y, He X, et al. Ag(2)S nanoparticle-mediated multiple ablations reinvigorates the immune response for enhanced cancer photo-immunotherapy. Biomaterials. 2021;264: 120451.
38. Qu S, Jia Q, Li Z, Wang Z, Shang LJSb. Chiral NIR-II fluorescent Ag2S quantum dots with stereospecific biological interactions and tumor accumulation behaviors. Sci Bull. 2022;67(12):1274–83.
39. Pan J, Wang Y, Zhang C, Wang X, Wang H, Wang J, et al. Antigen-directed fabrication of a multifunctional nanovaccine with ultrahigh antigen loading efficiency for tumor photothermal-immunotherapy. Adv Mater. 2018;30(8):1704408.

Publisher's Note